

ZIRCON RAMAN THERMOCHRONOLOGY: DATA VALUATION AND MEASUREMENT PROTOCOL

Birk Härtel^{*1}, Raymond Jonckheere¹, Lothar Ratschbacher¹

^{*} Contact: haertelb@mailserver.tu-freiberg.de

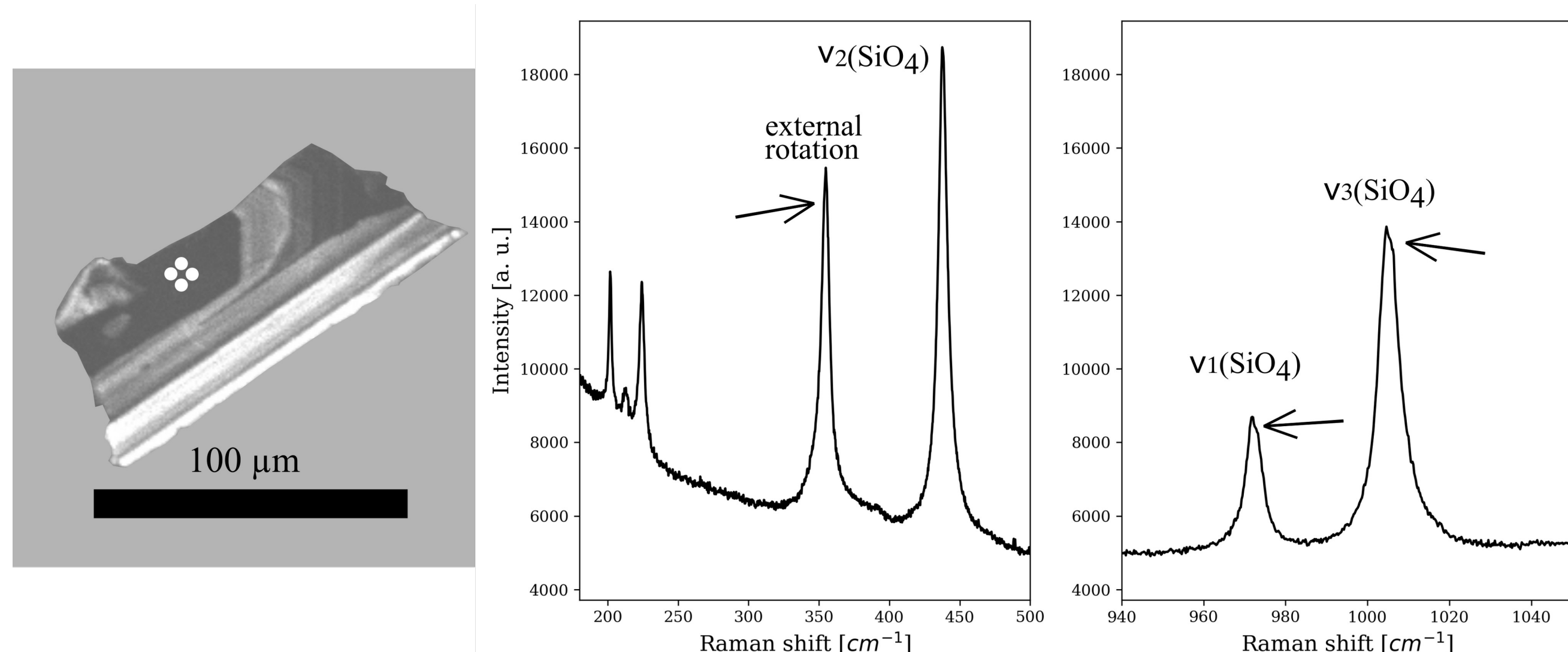


Fig. 1. CL image and Raman spectrum of a Tardree rhyolite zircon. The bands show asymmetric shapes (arrows) from band overlap, with exception of $v_2(\text{SiO}_4)$. The white dots in the CL images mark the Raman spots, with the spectrum being from the uppermost spot. Band overlap occurs despite the spots being in an apparently homogeneous zone. Band assignment after Kolesov et al. (2001).

BAND OVERLAP DETECTION

Zircon Raman dating requires the Raman spectrum of analyzed zircon to be free of artifacts. One example is the distortion of Raman band shapes by signal overlap from differently damaged zones (Fig. 1). This effect may be visible as band asymmetry and causes artificial broadening, leading to overestimation of radiation damage. The overlap affects the different bands differently (Fig. 2), with the narrow, strongly shifting $v_1(\text{SiO}_4)$, $v_3(\text{SiO}_4)$, and external rotation (ER) bands being strongly distorted, whereas $v_2(\text{SiO}_4)$ is only marginally affected. Multi-band Raman analysis allows to discriminate spectra exhibiting overlap by comparing damage estimates (D) from different bands (Fig. 3). Our for Tardree rhyolite (TDR, red) and Mogok Belt granite (M71, magenta) zircons affected by band overlap deviate from the expected relationship ($D_2 = D_3 = D_{\text{ER}}$) towards higher D_3 and D_{ER} values ($D_3 > D_{\text{ER}} > D_2$). Fig. 4 exploits the difference between D_3 and D_2 by plotting the D_3/D_2 ratio against D_2 and comparing the data with the prediction boundaries based on random measurement errors. The TDR and M71 data exhibiting band overlap lie outside the upper prediction boundary. These data are classified as broadened by overlap and may be excluded from further analysis.

PARTIAL ANNEALING

As for other thermochronological methods, the interpretation of zircon Raman ages depends on the thermal history of the dated sample. One aspect is the distinction of partial and complete annealing, marking the difference between mixed and reset ages (Wagner, 1981). For unannealed zircons, the measured radiation damage is equivalent to the zircon's α -dose ($D = D_\alpha$), but decreases with annealing.

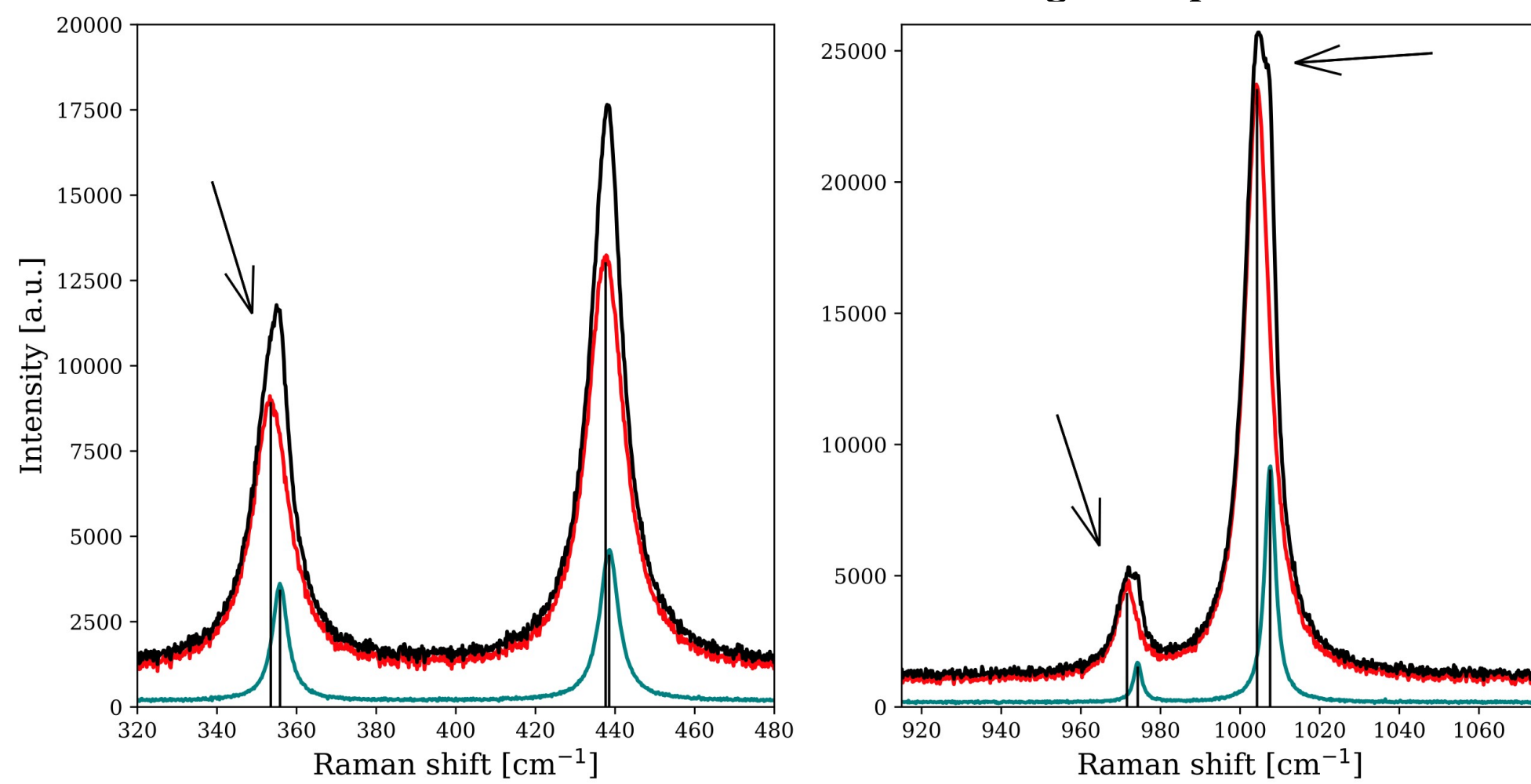


Fig. 2. Background-corrected spectra of two zircon grains at $D \sim 4 \cdot 10^{16} \alpha/\text{g}$ (teal) and $\sim 45 \cdot 10^{16} \alpha/\text{g}$ (red) and their sum (black). Vertical, gray lines indicate the band positions of the input spectra. Arrows mark visible deviations from the ideal band shape.

ACKNOWLEDGEMENTS

We thank Hideki Iwano and Masatsugu Ogasawara for providing the Duluth complex FC1 zircon separates and Jiří Sláma for the Plešovice zircon. The presented work is part of the doctoral project of Birk Härtel, supported by a scholarship of the German scholarship foundation (Studienstiftung des deutschen Volkes).

REFERENCES

Härtel, B., Jonckheere, R., Wauschkuhn, B., Hofmann, M., Frölich, S., and Ratschbacher, L.: Zircon Raman dating: Age equation and calibration. *Chem. Geol.*, **579**, 120351, 2021a. Härtel, B., Jonckheere, R., Wauschkuhn, B., and Ratschbacher, L.: The closure temperature(s) of zircon Raman dating. *Geochronology*, **3**, 259-272, 2021b. Kolesov, B.A., Geiger, C.A., and Armbruster, T.: The dynamic properties of zircon studied by single-crystal X-ray diffraction and Raman spectroscopy. *Eur. J. Mineral.*, **13**, 939-948, 2001. Wagner, G.A., 1981. Fission-track ages and their geological interpretation. *Nucl. Tracks* 5, 15-25. Sláma, J., Košler, J., Condon, D.J., Crowley, J.L., Gerdes, A., Hancher, J.M., Horstwood, M.S.A., Morris, G.A., Nasdala, L., Norberg, N., Schaltegger, U., Schoene, B., Tubrett, M.N., and Whitehouse, M.J., 2008. Plešovice zircon – A new natural reference material for U-Pb and Hf isotopic microanalysis. *Chem. Geol.* 249, 1-35.

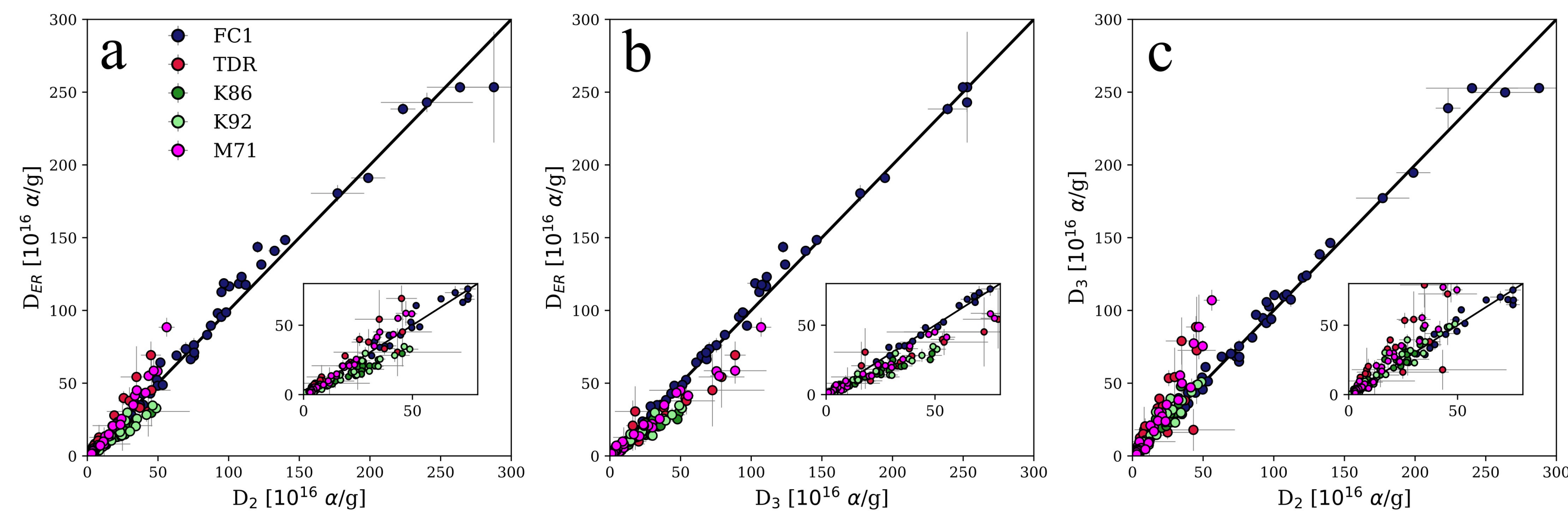


Fig. 3. D vs. D plots with D calculated from the $v_2(\text{SiO}_4)$, $v_3(\text{SiO}_4)$, and ER bandwidths using the calibration of Härtel et al. (2021a). The insets include the region up to $80 \cdot 10^{16} \alpha/\text{g}$ in detail. Error bars are 2σ . Some data of Tardree rhyolite (TDR) and Mogok Belt granite (M71) are affected by band overlap. The samples from the Katha range (K86 and K92) are partially annealed. Data from Duluth Complex FC1 are shown for comparison.

Some data from the Katha range samples plot outside the upper prediction boundary with both datasets being offset to values above 1. Samples showing this offset are classified as partially annealed.

APPLICATIONS AND MEASUREMENT PROTOCOL

D/D maps of single zircons are helpful to assess the feasibility of single-grain isochron dating, e.g. in sedimentary samples or samples containing few zircon grains, and evaluate the annealing state of and within the grain. Fig. 6 shows a CL image (a) and three Raman maps (b-d) of a Plešovice zircon grain (Sláma et al., 2008) with a core-rim zonation. The map of Γ_{ER} (b) shows the radiation-damage zonation with Raman bandwidths up to $\sim 40 \text{ cm}^{-1}$. In the D_3/D_2 map (c), several zones have elevated ratios and should thus not be targeted for zircon Raman dating. The D_2/D_{ER} map (d) shows ratios mainly between 0.8 and 1.3, indicating that no significant partial annealing has taken place during or after cooling of this zircon.

Fig. 7 shows a flow chart of zircon Raman dating, integrating the outlined evaluation steps into the measurement procedure for (1) detecting spectra with artificially broadened bands before measuring eU and (2) distinguishing between complete and partial annealing when interpreting the apparent zircon Raman age.

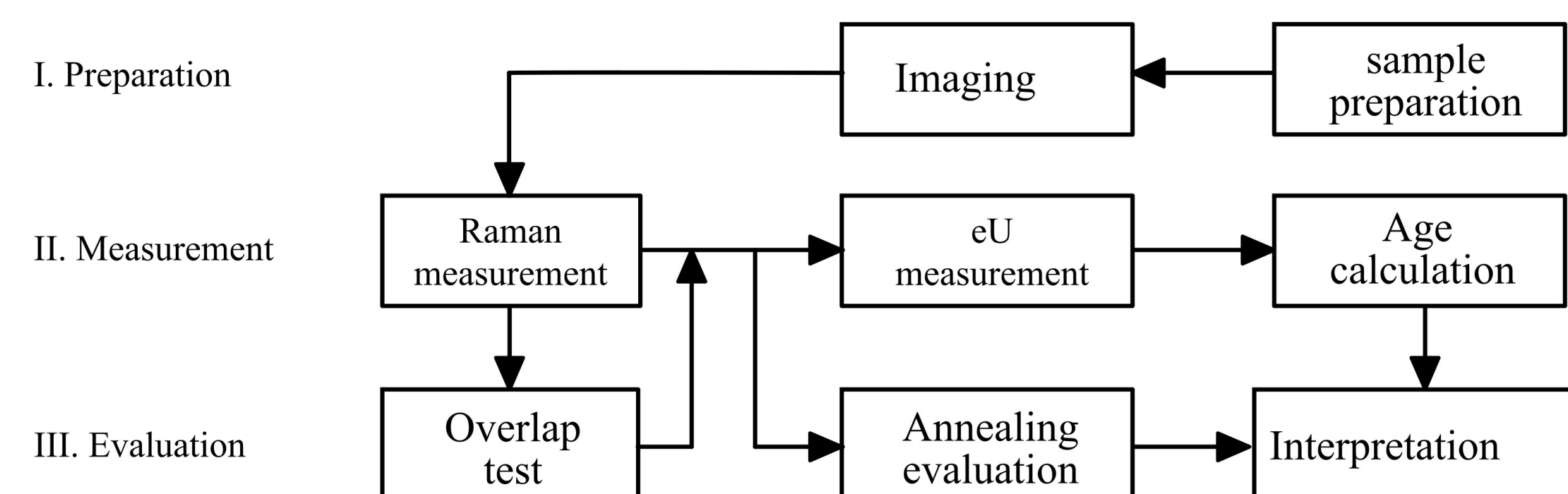


Fig. 7. Flow chart of a suggested zircon Raman dating procedure. The protocol consists of three steps: preparation, measurement, and evaluation. The overlap test helps to detect spectra containing artifacts that may be excluded from further analysis. The annealing evaluation is crucial for correctly interpreting the apparent zircon Raman age.

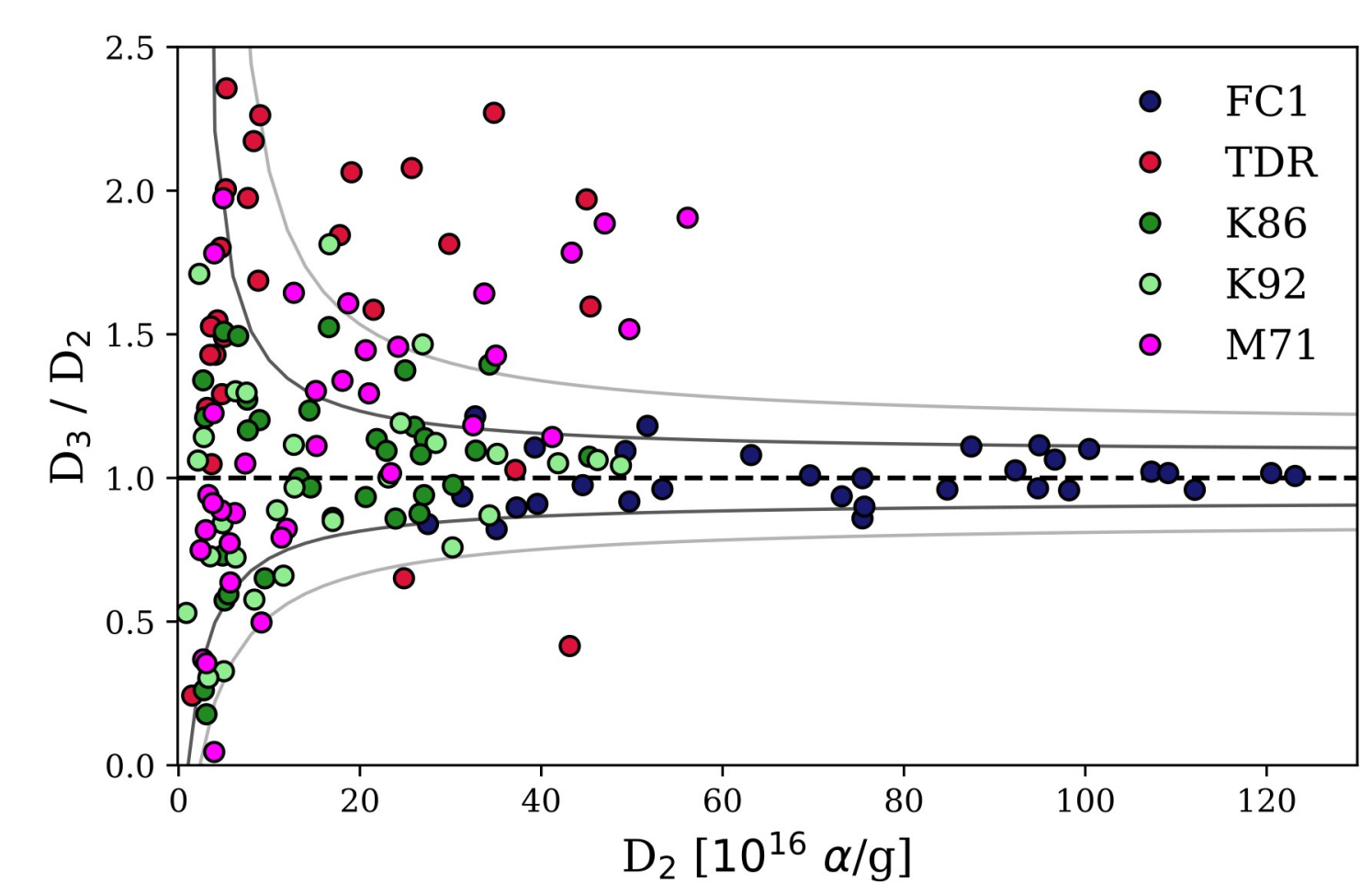


Fig. 4. Plots of D_3/D_2 vs. D_2 . The dashed line marks the expected value of 1 for well-behaved data. Prediction boundaries are included for 90 % (dark gray), and 99 % (light gray) of the data, assuming 4 % relative errors on Γ (1σ). The samples affected by overlap are the Tardree rhyolite (TDR) and the Mogok Belt granite (M71).

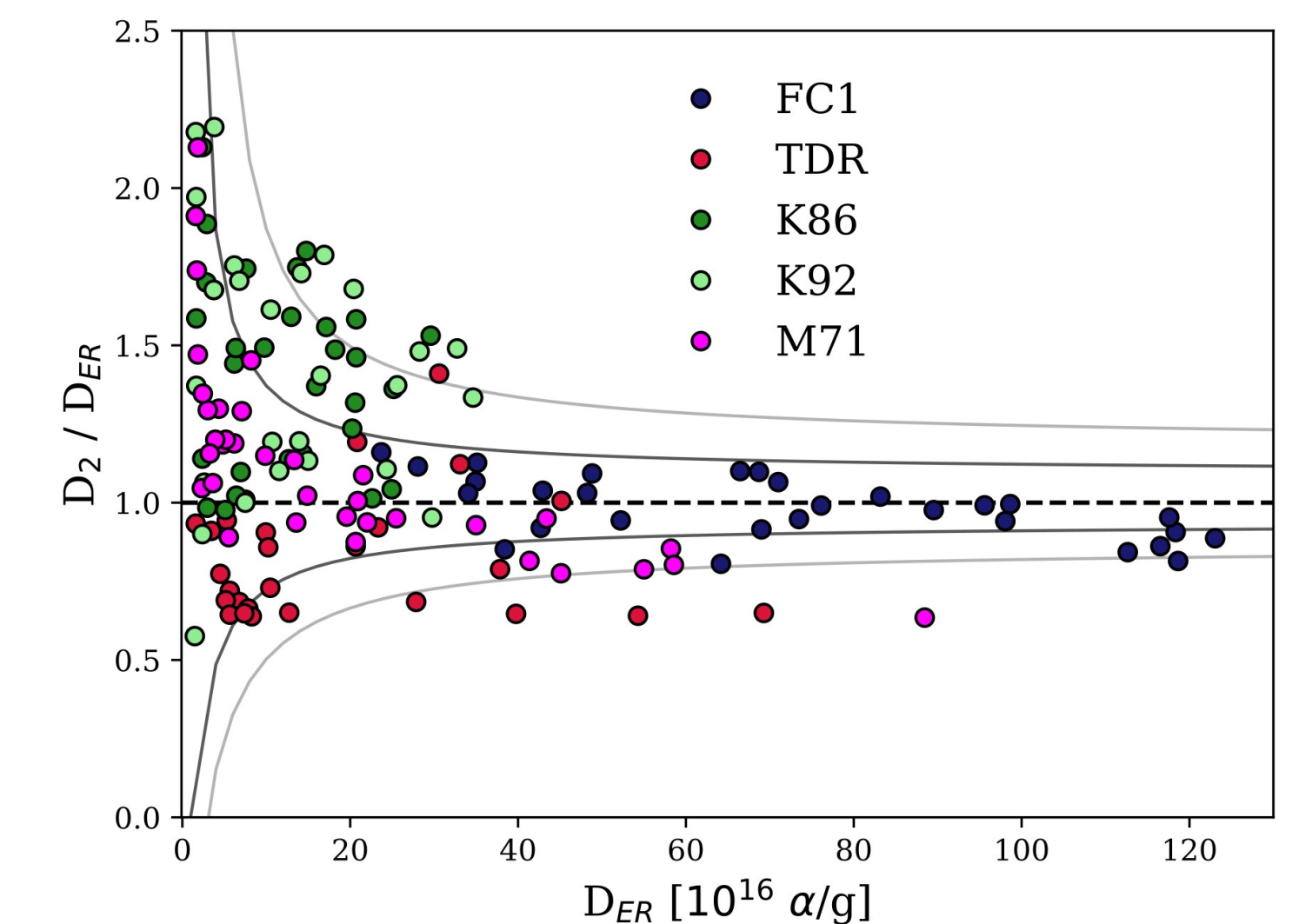


Fig. 5. Plots of D_3/D_2 vs. D_{ER} . The dashed line marks the expected value of 1 for unannealed or completely reset data. Prediction boundaries are included for 90 % (dark gray), and 99 % (light gray) of the data, assuming 4 % relative errors on Γ (1σ). The samples affected by partial annealing are the Katha range orthogneisses (K86 and K92).

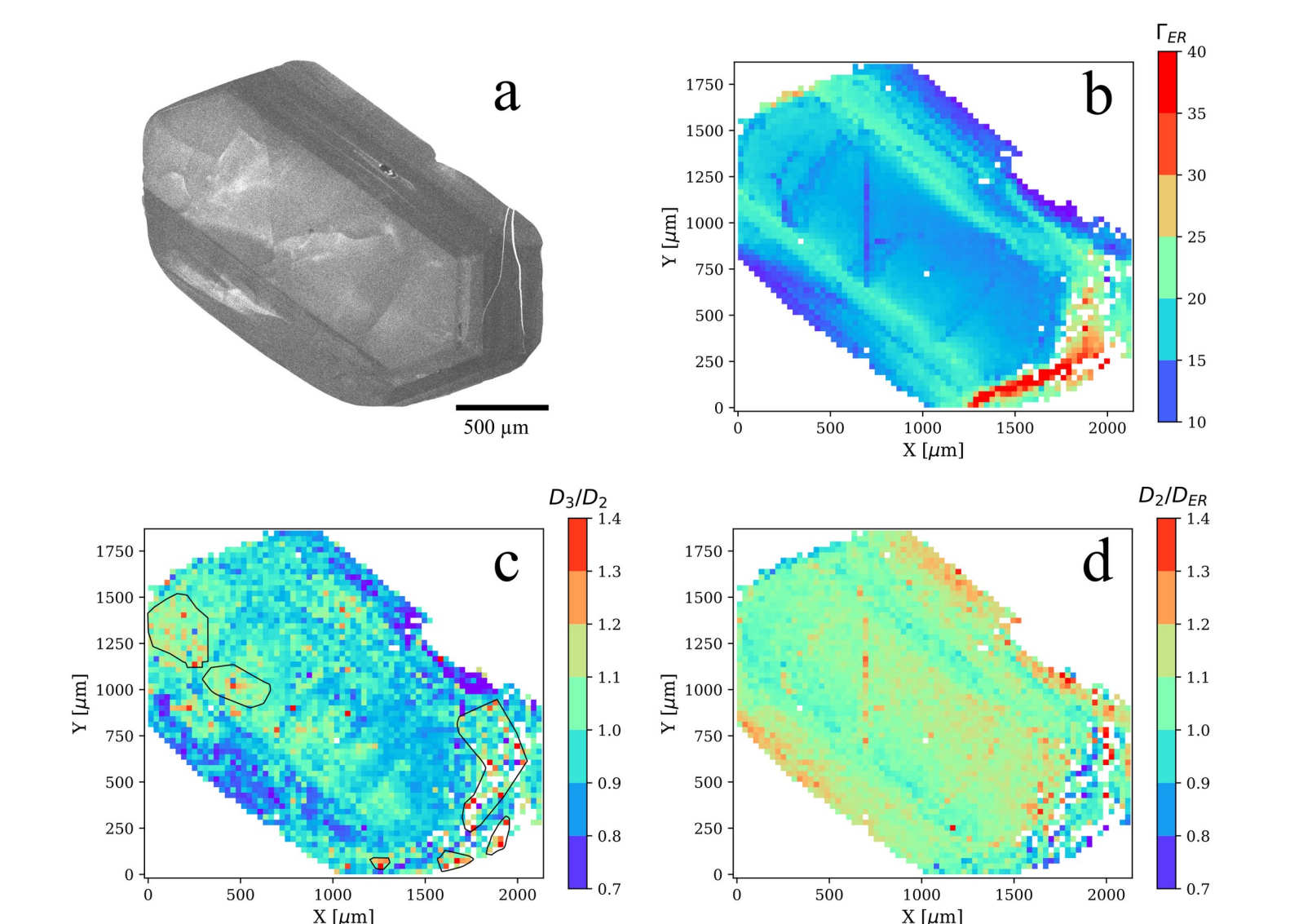


Fig. 6. CL and Raman images of a $3 \times 1 \text{ mm}$ Plešovice zircon. (a) CL image. (b) Raman map of Γ_{ER} indicating the degree of radiation damage. (c) Raman map of the D_3/D_2 ratio with areas showing band overlap encircled in black. (d) Raman map of the D_2/D_{ER} ratio. White pixels indicate measurement spots excluded due to low signal-to-noise ratio.